Supplementary Material

Analytical–numerical stress analysis and redesign of perforated backing plates in industrial diaphragm pumps: degradation of boundary conditions and optimal ligament configuration

Juan Gabriel Noa Águila [1], Yosbany Llody García [1], Reinier Jiménez Borges [1,*], Yoisdel Castillo Alvarez [2,*] and Ramón Quiza Sardiñas [3]

[1] Department of Mechanical Engineering, Universidad de Cienfuegos "Carlos Rafael Rodríguez", Cienfuegos 59430, Cuba

[2] Department of Mechanical Engineering, Universidad Tecnológica del Perú, Lima 15046, Peru

[3] Center for Advanced and Sustainable Manufacturing Studies, University of Matanzas, Matanzas 44740, Cuba

[*] Correspondence: reinier@ucf.edu.cu (R.J.B.); c19773@utp.edu.pe (Y.C.A.)

S1 Full radial finite element profiles of both plate faces

Figure S1 reports the complete radial profiles of the Von Mises equivalent stress obtained by the finite element simulation of Noa-Aguila et al. [21] for the original configuration ($d = 5$ mm, $p = 6.5$ mm), as referenced in Subsections 2.5 and 3.1 of the main text. The figure superimposes the two idealized analytical models (simply supported, SS; clamped, C) on the FEM profiles of the convex face (43 points) and the concave face (45 points). Two features are made explicit. First, along the smooth cross-center field the simply supported analytical model envelops the FEM response conservatively: its central maximum (267.98 MPa) exceeds the FEM convex-face peak (∼215 MPa) and the concave cross-center maximum (218.5 MPa) used as the calibration point. Second, the concave-face profile attains its absolute maximum (∼259 MPa) not at the center but in the perforated peripheral belt (hole-edge path), a local stress concentration that is, by construction, outside the scope of the first-order analytical model (assumption H5) and that is consistent with the location of the recurrent in-service fractures discussed in the main text.

S2 Extended parametric-sweep results

Table S1 extends Table 2 of the main text with two additional derived quantities for the eighteen geometrically feasible configurations: the relative variation of the maximum equivalent stress with respect to the installed configuration (positive values denote a reduction) and the operational safety factor under the simply supported model, $FS_{\mathrm{op}}^{\mathrm{SS}} = \sigma_y/\sigma_{\mathrm{eq,max}}^{\mathrm{SS}}$, computed with the experimentally verified yield strength $\sigma_y = 195$ MPa. The curvature factors f_c^{SS} and f_c^{C} are constant across the sweep (the macroscopic cap geometry $R = 172$ mm, $R_0 = 560$ mm, $h = 13$ mm does not change) and are therefore not tabulated per configuration. Only configurations 3, 2, 6 and 9 reduce the maximum stress relative to the installed design.

S3 Point-by-point finite element calibration

The analytical model is calibrated against the FEM response of the installed configuration [21] following the procedure summarized below, as referenced in Subsections 2.5, 3.5 and 4.2 of the main text. The dimensionless boundary-degradation parameter η_{BC} locates the FEM concave cross-center

Table S1: Extended parametric-sweep results for the eighteen configurations: ligament efficiency, maximum Von Mises equivalent stress under the simply supported (SS) and clamped (C) models, relative stress variation with respect to the installed configuration (positive = reduction), and operational safety factor under the simply supported model ($FS_{\mathrm{op}}^{\mathrm{SS}} = \sigma_y/\sigma_{\mathrm{eq,max}}^{\mathrm{SS}}$, $\sigma_y = 195$ MPa).

Conf.	d **(mm)**	p **(mm)**	t_{lig} **(mm)**	η **(–)**	$\sigma_{\mathrm{eq,max}}^{\mathrm{SS}}$ **(MPa)**	$\sigma_{\mathrm{eq,max}}^{\mathrm{C}}$ **(MPa)**	**Var.**	$FS_{\mathrm{op}}^{\mathrm{SS}}$ **(%)**
1	5	6.5	1.5	0.231	267.98	105.49	+0.0	0.728
2	5	7.0	2.0	0.286	209.28	82.34	+21.9	0.932
3	5	7.5	2.5	0.333	172.25	67.73	+35.7	1.132
4	6	7.0	1.0	0.143	441.60	173.95	-64.8	0.442
5	6	7.5	1.5	0.200	307.27	120.98	-14.7	0.635
6	6	8.0	2.0	0.250	237.25	93.37	+11.5	0.822
7	7	8.0	1.0	0.125	502.81	198.12	-87.6	0.388
8	7	8.5	1.5	0.176	346.24	136.37	-29.2	0.563
9	7	9.0	2.0	0.222	265.02	104.33	+1.1	0.736
10	8	9.0	1.0	0.111	563.71	222.20	-110.4	0.346
11	8	9.5	1.5	0.158	384.95	151.66	-43.6	0.507
12	8	10.0	2.0	0.200	292.64	115.24	-9.2	0.666
13	9	10.0	1.0	0.100	624.33	246.21	-133.0	0.312
14	9	10.5	1.5	0.143	423.44	166.88	-58.0	0.461
15	9	11.0	2.0	0.182	320.15	126.11	-19.5	0.609
16	10	11.0	1.0	0.091	684.72	480.36†	-155.5	0.285
17	10	11.5	1.5	0.130	461.73	182.05	-72.3	0.422
18	10	12.0	2.0	0.167	347.59	136.97	-29.7	0.561

Note: Var. (%) $= 100\,(\sigma_{\mathrm{eq,max}}^{\mathrm{SS},(1)} - \sigma_{\mathrm{eq,max}}^{\mathrm{SS},(\mathrm{i})})/\sigma_{\mathrm{eq,max}}^{\mathrm{SS},(1)}$ relative to the installed configuration 1; positive values denote a stress reduction. † For configuration 16 the clamped-model maximum relocates to the plate edge.

maximum ($\sigma_{\mathrm{FEM}} = 218.5$ MPa) within the interval bounded by the clamped and simply supported analytical predictions for configuration 1:

$$\eta_{\mathrm{BC}} = \frac{\sigma_{\mathrm{FEM}} - \sigma_{\mathrm{eq,max}}^{\mathrm{C},(1)}}{\sigma_{\mathrm{eq,max}}^{\mathrm{SS},(1)} - \sigma_{\mathrm{eq,max}}^{\mathrm{C},(1)}} = \frac{218.5 - 105.49}{267.98 - 105.49} = 0.695. \tag{S1}$$

The simply supported model overestimates the FEM value by $(267.98 - 218.5)/218.5 = 22.6\%$, whereas the clamped model underestimates it by $(105.49 - 218.5)/218.5 = -51.7\%$; the value $\eta_{\mathrm{BC}} = 0.695$ therefore places the physical response at 69.5% of the range toward the simply supported case and supports the use of that model as a conservative screening bound. The absolute calibration is applied as a single global positive scale factor,

$$k = \frac{\sigma_{\mathrm{FEM}}}{\sigma_{\mathrm{eq,max}}^{\mathrm{SS},(1)}} = \frac{218.5}{267.98} = 0.8154, \qquad \hat{\sigma}_{\mathrm{FEM}}^{(i)} = k\,\sigma_{\mathrm{eq,max}}^{\mathrm{SS},(\mathrm{i})}, \tag{S2}$$

which, being identical for every configuration, rescales all predictions without altering their relative ordering. Table S2 reports the calibrated stress estimate and the resulting effective safety factor $FS_{\mathrm{eff}} = \sigma_y/\hat{\sigma}_{\mathrm{FEM}}$ for the installed configuration and the four configurations that reduce the maximum stress. The calibrated value for the installed plate, $FS_{\mathrm{eff}}^{(1)} = 195/218.5 = 0.89$, reproduces the operational safety factor reported in the main text.

Table S2: Point-by-point FEM calibration of the installed configuration and the four stress-reducing candidates: maximum stress under the simply supported model, calibrated estimate $\hat{\sigma}_{\mathrm{FEM}} = k\,\sigma^{\mathrm{SS}}_{\mathrm{eq,max}}$ with $k = 0.8154$, and effective safety factor $FS_{\mathrm{eff}} = \sigma_y/\hat{\sigma}_{\mathrm{FEM}}$ ($\sigma_y = 195$ MPa).

Configuration	$\boldsymbol{\sigma^{\mathrm{SS}}_{\mathrm{eq,max}}}$ **(MPa)**	$\hat{\boldsymbol{\sigma}}_{\mathbf{FEM}}$ **(MPa)**	$\boldsymbol{FS_{\mathrm{eff}}}$
1 (installed)	267.98	218.5	0.89
3 (candidate)	172.25	140.4	1.39
2	209.28	170.6	1.14
6	237.25	193.4	1.01
9	265.02	216.1	0.90

Note: The effective safety factor and the calibrated stress are model-based estimates conditional on the linear-scaling assumption; the relative ranking of configurations is independent of k. The direct finite element verification campaign reported in Subsection 3.6 of the main text (Table 6) shows that the linear-scaling assumption is not supported for absolute magnitudes: the calibrated estimates of this table are retained for documentation of the screening stage and are superseded, for configurations 1–3, by the directly computed values.

S4 Model assumptions of the analytical formulation

For completeness, the assumptions underlying the closed-form analytical model (Subsection 2.3 of the main text) are consolidated below.

H1. The plate is idealized as a shallow spherical cap with ratio $h/R \approx 0.076$, satisfying the applicability criterion of classical thin-plate theory ($h/R < 1/10$).

H2. The material is homogeneous, isotropic and linearly elastic within the considered regime, verified a posteriori by confirming that the predicted maximum stresses remain below the conventional yield strength.

H3. The load is static and uniformly distributed over the entire concave surface; the implications under the actual cyclic regime are discussed in the main text.

H4. The physical stepped clamping is modeled through two idealized comparison cases: simply supported edge and clamped edge.

H5. Local stress concentrations at the edges of individual holes are considered beyond the scope of the first-order analytical model and are attributed to numerical simulation for detailed characterization.

These assumptions delimit the validity of the screening model: H1–H4 define the smooth-field elastic solution used for the relative ranking, while H5 explicitly excludes the local hole-edge concentration, which is precisely the feature responsible for the concave-face peak shown in Figure S1.

S5 Photographic evidence of the PMI material identification campaign

This section documents the experimental campaign of Subsection 2.2 of the main text. Figure S2 shows the portable optical emission spectrometry probe applied directly on the backing plate removed from service, with the argon-shielded arc visible at the measurement spot. Figure S3 shows

the instrument analysis screen with the argon-shielded burns, the element-by-element averages reported in Table 1 of the main text (sample identified as "Plato Respaldo Ac. Inox. Argon"), and the resulting grade verdict (1.4310 X10CrNi18-8) displayed by the instrument. Figure S4 shows the grade-matching dialog, listing 1.4310 X10CrNi18-8 as the primary match [1/7] against the candidate austenitic family (1.4301, 1.4541, 1.4550, 1.4944, 1.4948 and St52.0S). Figure S5 shows the overall measurement scene on the component.

S6 Direct finite element verification campaign: mesh summary and contour plots

This section documents the verification campaign of Subsections 2.6 and 3.6 of the main text. Table S3 summarizes the three solved models: mesh statistics, exported surface nodes per face, global maximum equivalent stress, its location, and maximum total deformation.

Table S3: Summary of the direct finite element verification campaign (ANSYS Mechanical 2025 R2; tetrahedral mesh, program-controlled adaptive sizing, one adaptive refinement loop; fixed support on the annular step, $P = 3$ MPa on the concave face; $E = 200$ GPa, $\nu = 0.3$).

	Conf. 1 (5×6.5)	**Conf. 2** (5×7.0)	**Conf. 3** (5×7.5)
Nodes (model)	261,578	230,159	205,679
Elements (model)	131,614	117,032	105,566
Exported nodes, concave face	44,491	38,381	33,657
Exported nodes, convex face	44,957	38,861	34,100
Global $\sigma_{\mathrm{eq,max}}$ (MPa)	338.18	290.81	261.48
Location of global maximum	Concave face, perforated peripheral belt		
Maximum total deformation (mm)	0.332	0.310	0.294

The three meshes are of comparable density (205,679–261,578 nodes), the global maximum is located on the concave face within the perforated peripheral belt in every case, and the maximum total deformations remain below 2.6% of the plate thickness, consistent with the linear-elastic idealization. Figures S6–S8 show the corresponding Von Mises equivalent stress contours of the loaded (concave) face at full load ($t = 1$ s), with per-configuration auto-ranged legend scales (the quantitative comparison between configurations is provided in Figure 8 and Table 6 of the main text); in the three contours, the highest-stress band is visually concentrated in the peripheral belt, while the central region remains in the low range of the scale. The complete nodal fields of both faces (equivalent stress and total deformation) are provided as Dataset S1, and the processed radial envelope profiles of the cross-center and hole-edge series, together with the campaign master table, as Dataset S2.

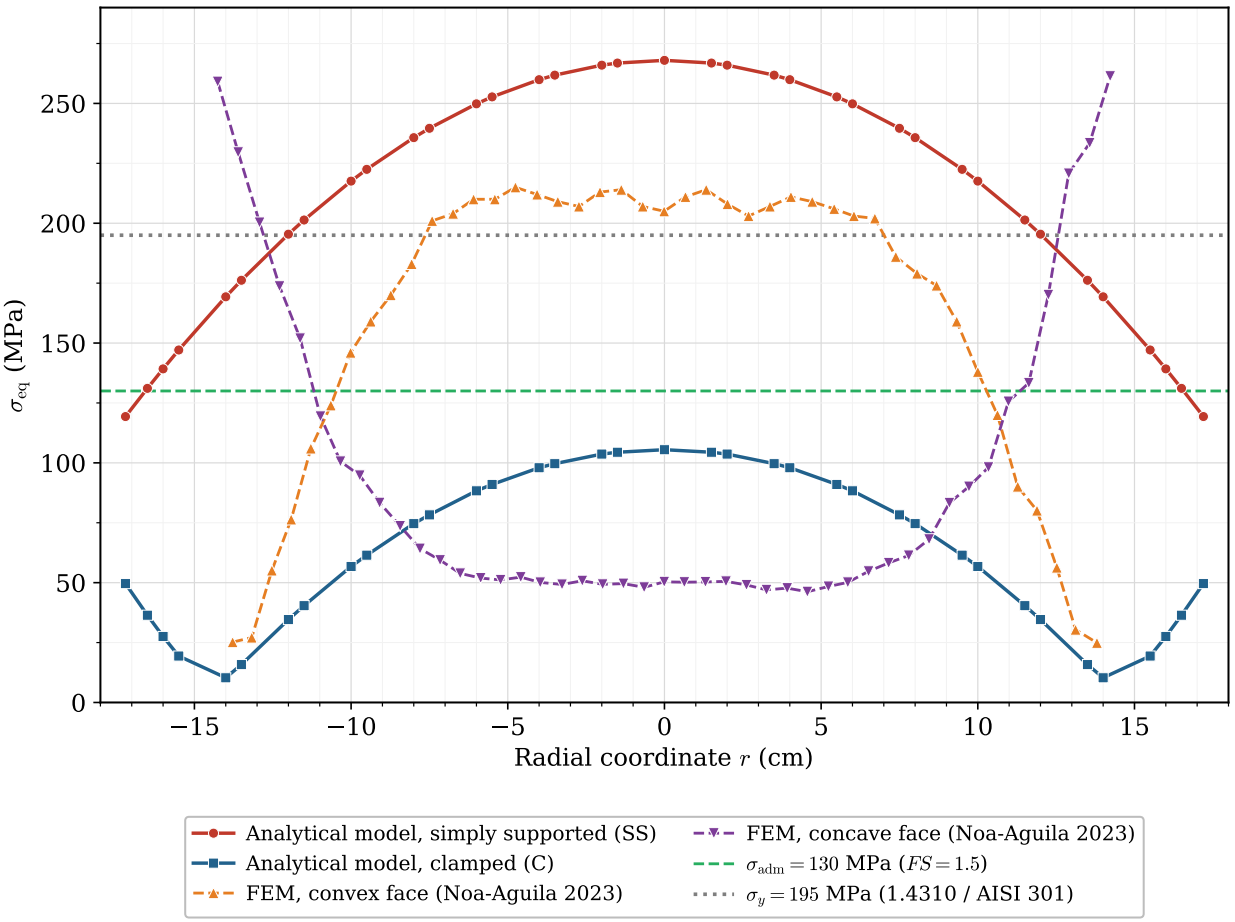


Figure S1: Radial distribution of the Von Mises equivalent stress for the original configuration ($d = 5$ mm, $p = 6.5$ mm): analytical simply supported (SS) and clamped (C) models compared with the full FEM radial profiles of the convex face (43 measurement points) and the concave face (45 measurement points) reported by Noa-Aguila et al. [21]. The green dashed line indicates the allowable stress $\sigma_{\text{adm}} = 130$ MPa ($FS = 1.5$ over $\sigma_y = 195$ MPa); the gray dotted line indicates the yield strength. The simply supported model envelops the smooth cross-center field, whereas the concave-face maximum in the peripheral belt (∼259 MPa, hole-edge path) corresponds to the local stress concentration excluded from the first-order model (assumption H5).

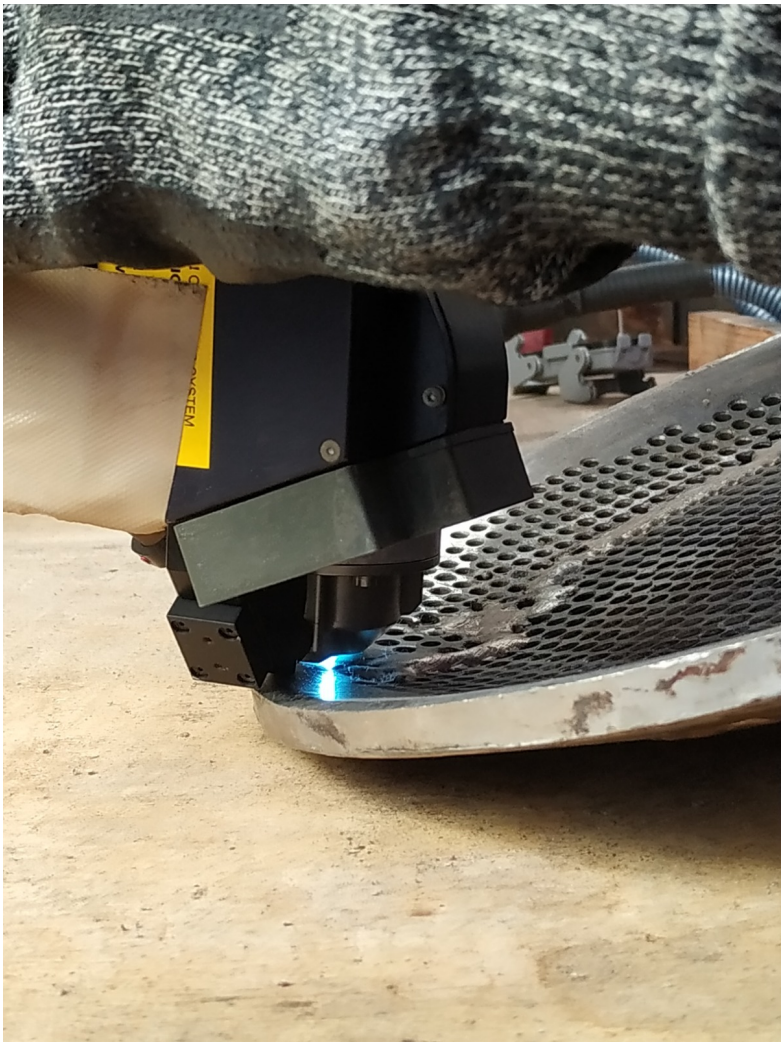


Figure S2: PMI probe applied on the perforated backing plate removed from service; the argon-shielded arc is visible at the measurement spot on the prepared surface.

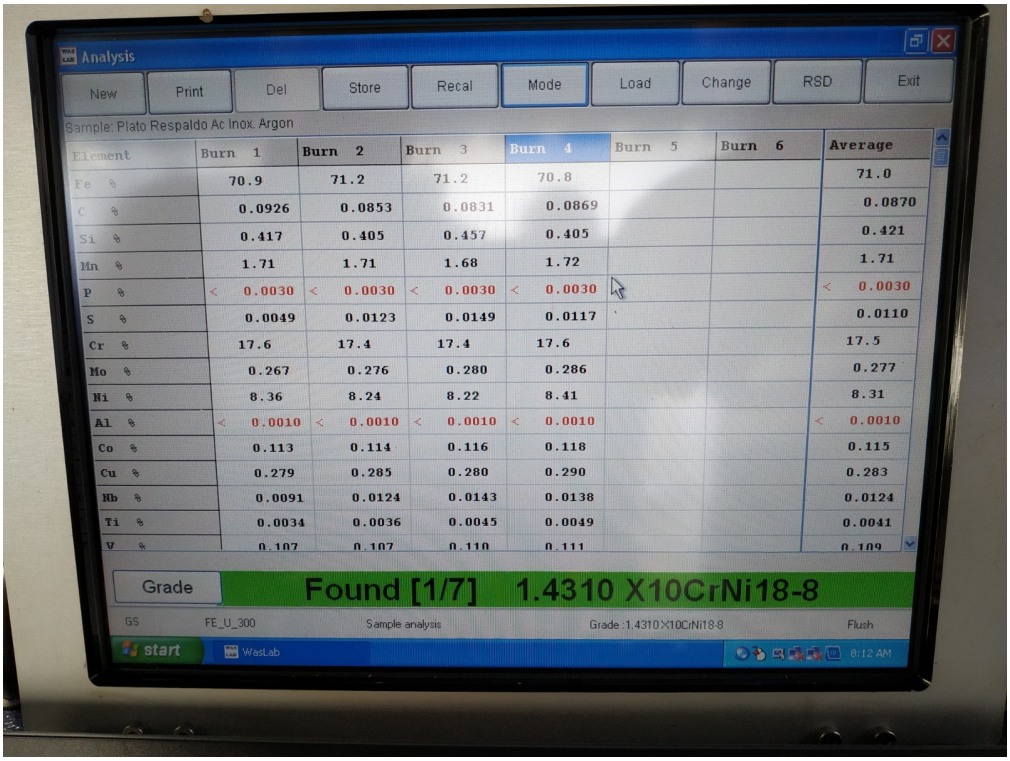


Figure S3: Instrument analysis screen showing the argon-shielded burns, the element-by-element averages (Fe 71.0, C 0.0870, Si 0.421, Mn 1.71, Cr 17.5, Ni 8.31, Mo 0.277 % wt) reported in Table 1 of the main text, and the grade verdict 1.4310 X10CrNi18-8 displayed by the instrument.

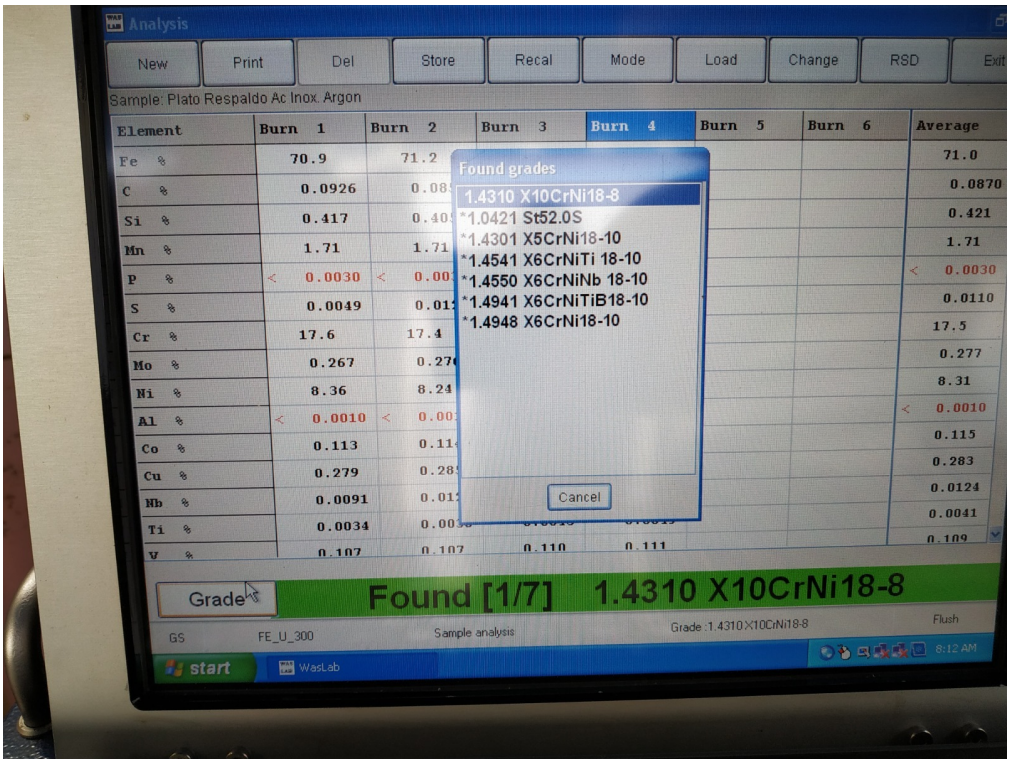


Figure S4: Grade-matching dialog of the instrument: 1.4310 X10CrNi18-8 is returned as the primary match [1/7] against the candidate designations (1.4301, 1.4541, 1.4550, 1.4944, 1.4948, St52.0S).

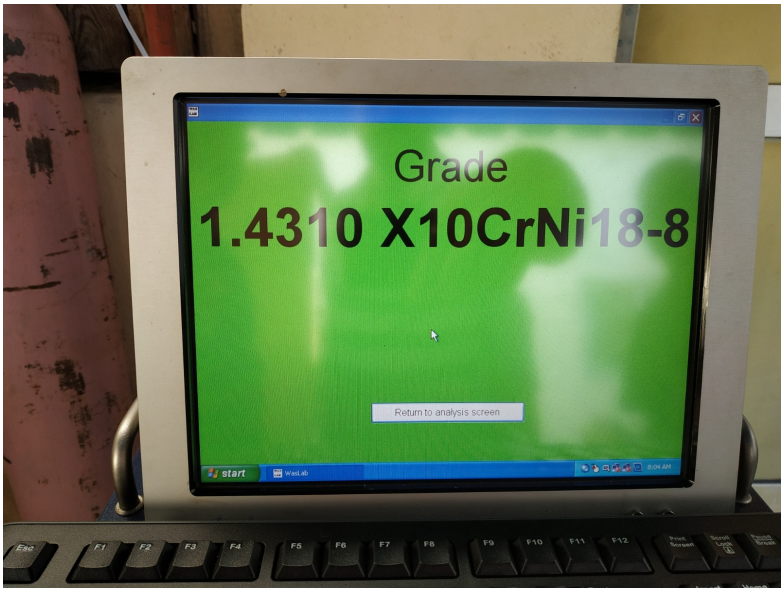


Figure S5: Overall view of the measurement campaign on the backing plate removed from service, with the prepared measurement spot on the perforated surface.

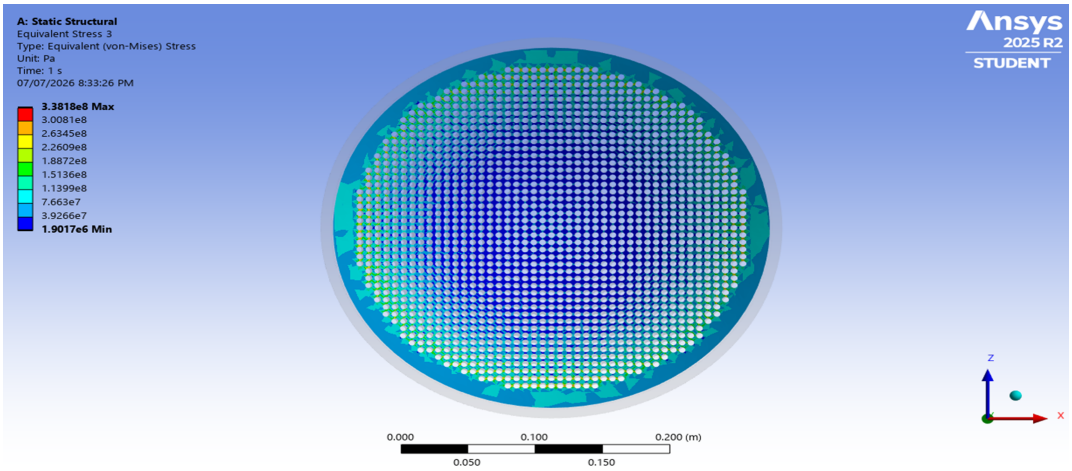


Figure S6: Von Mises equivalent stress contour of the concave (loaded) face, configuration 1 (5×6.5, installed), at full load. Legend scale auto-ranged for this configuration; see Figure 8 of the main text for the quantitative comparison.

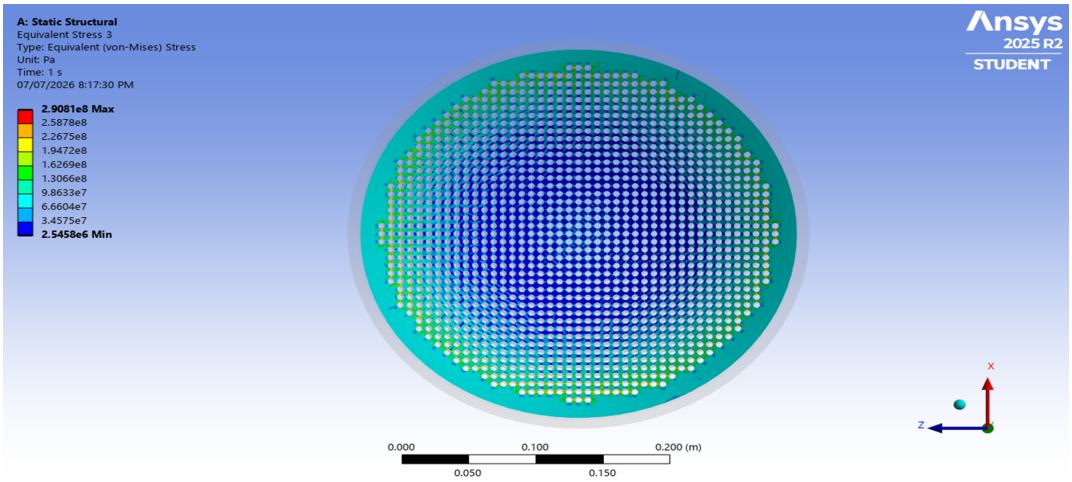


Figure S7: Von Mises equivalent stress contour of the concave (loaded) face, configuration 2 (5×7.0), at full load. Legend scale auto-ranged for this configuration; see Figure 8 of the main text for the quantitative comparison.

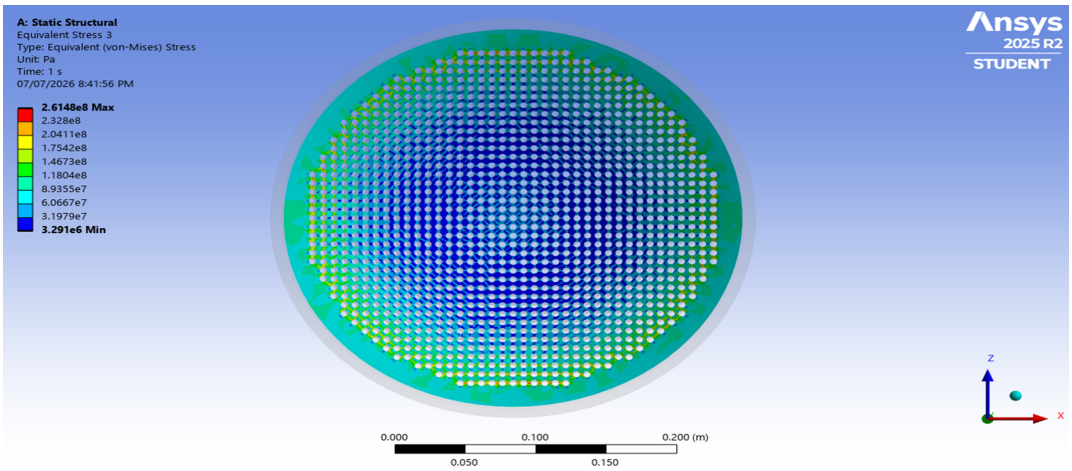


Figure S8: Von Mises equivalent stress contour of the concave (loaded) face, configuration 3 (5×7.5, redesign candidate), at full load. Legend scale auto-ranged for this configuration; see Figure 8 of the main text for the quantitative comparison.